© 2023. Published by The Company of Biologists Ltd | Journal of Cell Science (2023) 136, jcs260182. doi:10.1242/jcs.260182

RESEARCH ARTICLE

STAT3 signaling induced by the IL-6 family of cytokines modulates angiogenesis

Julian Rapp[1], Malte Jung[1], Rhena F. U. Klar[2], Julian Wolf[1], Jakob Arnold[1], Oliver Gorka[3], Olaf Groß[3,4,5], Clemens Lange[1,6], Hansjürgen Agostini[1], Günther Schlunck[1] and Felicitas Bucher[1,*]

ABSTRACT

Aberrant angiogenesis is a hallmark of cardiovascular and retinal neovascular disease. The STAT3 signaling pathway represents a potential pharmacological target for these diseases due to its impact on angiogenesis. Surprisingly, some STAT3 activators, such as the IL-6 cytokine family member oncostatin M (OSM), enhance angiogenesis, whereas others, such as ciliary neurotropic factor (CNTF), reduce it. This study aimed to clarify these conflicting effects. In contrast to the anti-angiogenic cytokine CNTF, the pro-angiogenic cytokine OSM was able to activate intracellular signaling pathways beyond the STAT3 pathway, including the ERK and AKT pathways. These differences translated into transcriptomic and metabolic shifts. siRNA-mediated STAT3 knockdown experiments showed a decrease in VEGF-induced endothelial migration and sprouting, enhancing the pro-angiogenic drive of OSM and switching the CNTF response from anti-angiogenic to pro-angiogenic. These effects correlated with a transcriptomic shift representing enhanced STAT1 and ERK activity following STAT3 knockdown, including a compensatory prolonged phosphorylated STAT1 activity. In conclusion, the angiogenic effect of STAT3 appears to be determined by cytokine-induced STAT3 specificity and simultaneous activity of other intracellular signaling pathways, whereas the STAT3 pathway, predominantly recognized for its pro-angiogenic phenotypes, reveals novel anti-angiogenic potential.

KEY WORDS: Angiogenesis, Endothelial cell, STAT3, IL-6 family cytokines, Oncostatin M, Ciliary neurotrophic factor

INTRODUCTION

Angiogenesis is a complex process that is critical to physiological development as well as disease progression. It plays a key role in macrovascular as well as microvascular diseases including arteriosclerosis (Camaré et al., 2017), stroke (Navaratna et al., 2009; Deveza et al., 2012) and diabetic retinopathy (Crawford et al., 2009). Moreover, tumors tend to stimulate angiogenesis to fuel their need of metabolites for uninhibited growth (Viallard and Larrivée, 2017). Targeting angiogenesis hence represents an important therapeutic approach. Understanding the underlying mechanisms of angiogenesis on a molecular level is a crucial prerequisite for the basis of identifying novel therapeutic targets.

Vascular endothelial growth factor (VEGF or VEGFA) is to date the most prominent cytokine that regulates angiogenic processes in disease (Melincovici et al., 2018). However, a deeper understanding of the pathomechanisms behind specific diseases such as arteriosclerosis and retinal neovascular disease has revealed that inflammatory processes also modulate angiogenesis (Dan-Brezis et al., 2019; Wolf and Ley, 2019). Among others, the interleukin 6 (IL-6) cytokine family plays a key role in mediating inflammatory responses and shows potential to modify inflammation-induced angiogenesis (Zhang et al., 2015; Jones and Jenkins, 2018).

The IL-6 cytokine family consists of multiple cytokines, including IL-6, ciliary neurotrophic factor (CNTF) and oncostatin M (OSM). They all bind to a similar receptor complex, share intracellular signaling pathways and ultimately share downstream targets as well (Heinrich et al., 2003). All IL-6 cytokines signal through the gp130 (IL6ST)-mediated recruitment of receptor-associated Janus kinases (JAKs), which leads to phosphorylation and therefore activation of signal transducer and activator of transcription (STAT) proteins, especially STAT3 (Heinrich et al., 2003; Jones and Jenkins, 2018). STAT3 was often reported to promote tumor growth (Johnson et al., 2018; Hu et al., 2019) and angiogenesis (Jung et al., 2005). However, the effects of IL-6 family cytokines on angiogenesis are inconsistent, despite their shared activation of the STAT3 signaling pathway (Vasse et al., 1999; Bucher et al., 2016, 2020).

Recent studies on CNTF suggest an anti-angiogenic effect of CNTF-induced STAT3 signaling on vascular endothelial cells and retinal angiogenesis (Bucher et al., 2016, 2020). CNTF activates STAT3 by binding to a heterotrimeric receptor complex consisting of gp130, LIF-receptor β (LIFRβ) and the CNTF receptor α (CNTFRα). Interestingly, only a few cell types, such as neurons and skeletal muscle cells, express CNTFRα (Davis et al., 1991), but a soluble CNTFRα enables other cell types, including vascular endothelial cells, to respond to CNTF signaling (Davis et al., 1993).

In contrast to CNTF, OSM elicits a pro-angiogenic response in vascular endothelial cells (Vasse et al., 1999), enhances tumor progression (Zhu et al., 2015) and is associated with cardiovascular disease (Modur et al., 1997; Abe et al., 2019). OSM-induced intracellular signaling hence represents a potential target for new therapeutic approaches in neovascular disease (Kucia-Tran et al., 2018). Receptors necessary for OSM signaling, gp130 and OSMRβ, are widely distributed among different cell types (Richards, 2013), causing OSM to not only influence diseases related to angiogenic processes but also other diseases, including diseases associated with bone remodeling, lung fibrosis or inflammatory skin conditions (Richards, 2013).

[1]Eye Center, Medical Center – University of Freiburg, Faculty of Medicine, University of Freiburg, 79106 Freiburg, Germany. [2]Department of Medicine I, Medical Center – University of Freiburg, Faculty of Medicine, University of Freiburg, 79106 Freiburg, Germany. [3]Institute of Neuropathology, Medical Center – University of Freiburg, Faculty of Medicine, University of Freiburg, 79106 Freiburg, Germany. [4]Signalling Research Centres BIOSS and CIBSS, University of Freiburg, 79104 Freiburg, Germany. [5]Center for Basics in NeuroModulation (NeuroModulBasics), Faculty of Medicine, University of Freiburg, 79106 Freiburg, Germany. [6]Ophtha-Lab, Department of Ophthalmology, St. Franziskus Hospital Muenster, 48145 Muenster, Germany.

*Author for correspondence (felicitas.bucher@uniklinik-freiburg.de)

J.R., 0000-0001-6770-8116; F.B., 0000-0003-0081-1420

Handling Editor: Daniel Billadeau
Received 5 May 2022; Accepted 21 November 2022

Journal of Cell Science (2023) 136, jcs260182. doi:10.1242/jcs.260182

The reported inverse angiomodulatory effect of CNTF and OSM on vascular endothelial cells, despite them sharing STAT3 signaling as the predominant intracellular signaling pathway, underlines that more research is needed to fully understand all aspects of cytokine-induced STAT3 signaling. Using *in vitro* angiogenesis models, we confirmed that OSM enhances vascular endothelial cell migration and sprouting, whereas CNTF limits VEGF-induced endothelial sprouting. The degree of STAT3 specificity correlated with the angiogenic phenotype, whereas STAT3 knockdown experiments suggested that the effect of STAT3 signaling on angiogenesis is highly context dependent and can result in pro- and anti-angiogenic reactions. A detailed understanding of STAT3 activity in disease is therefore necessary to successfully use STAT3 as therapeutic target.

RESULTS

OSM and CNTF have opposite angiomodulatory effects on vascular endothelial cells

To evaluate the effect of OSM and of CNTF co-stimulated with its soluble receptor CNTFRα (CNTF+R) on angiogenesis *in vitro*, both cytokines were tested in the spheroid-sprouting assay, the scratch-wound assay and proliferation assay. OSM treatment provided a strong pro-angiogenic stimulus on vascular endothelial sprouting (25% increase) compared to the basal sprouting rate [endothelial basal medium (EBM) control group]. An additional pro-angiogenic impulse of 31% on top of VEGF-induced sprouting (VEGF control group) was induced after OSM+VEGF stimulation (Fig. 1A). In contrast, CNTF+R significantly reduced VEGF-initiated sprouting by 21.9% (Fig. 1A).

In the scratch-wound assay, OSM treatment significantly enhanced endothelial migration after 10 h by 28.4% compared to that of the EBM control (Fig. 1B). Interestingly, the OSM-induced pro-migratory stimulus surpassed the VEGF-induced effect within the first 10 h but stagnated afterwards, whereas VEGF showed a consistent wound-closing kinetic. In line with the observation in the spheroid-sprouting assay, after 10 h, OSM+VEGF significantly enhanced endothelial cell migration by 29.3% in comparison to VEGF alone (Fig. 1B). In contrast, CNTF+R did not affect migration significantly with or without VEGF (Fig. 1B). Similar effects were seen with regards to cell proliferation: OSM significantly increased cell proliferation by 63.7% compared to that seen in the EBM control and by 55.3% on top of VEGF-induced proliferation (Fig. 1C). As before, CNTF+R with or without VEGF did not achieve a significant effect on cell proliferation.

OSM, in contrast to CNTF+R, activates intracellular signaling pathways beyond STAT3

We hypothesized that the observed divergent effects of OSM and CNTF+R on endothelial cells correlated with distinct intracellular signaling patterns. Western blot analysis showed that OSM and CNTF+R both activated the STAT3 signaling pathway in human umbilical vein endothelial cells (HUVECs) by phosphorylating the Tyr705 site of STAT3 (pSTAT3, Tyr705), but only OSM was able to activate phosphorylation of the Ser727 site (pSTAT3, Ser727) (Fig. 2A). STAT1 activation, as indicated by levels of phosphorylated (p) STAT1 (pSTAT1) upon exposure to cytokines, was the most prominent after OSM treatment, whereas CNTF+R led to a very weak pSTAT1 response (Fig. 2A). STAT5 (STAT5A) activation was not evident for either cytokine (Fig. 2A). Co-stimulation with VEGF led to the same results (Fig. 2A). In contrast to CNTF+R, OSM also led to activation of other pathways including ERK and AKT, represented by the increase in pERK and pAKT levels in response to OSM treatment (Fig. 2B), which was especially stable in the presence of VEGF (Fig. 2B).

To screen for an explanation of these different signaling patterns between OSM and CNTF+R, we further analyzed more upstream-located proteins in the signaling cascade by measuring phosphorylation of JAKs. Interestingly, OSM and CNTF+R with or without VEGF co-stimulation did not generate a pJAK1 or pJAK2 signal in protein lysates after 5 min of stimulation, but only OSM was able to introduce a statically significant pTYK2 activation (Fig. S1A).

The time course of the intracellular signaling pathways revealed that both OSM as well as CNTF+R rapidly increased pSTAT3 levels, peaking at approximately 15 min, with a more prolonged activation observed for OSM (Fig. S1B). ERK signaling induced by OSM appeared more rapid and stronger, but of shorter duration than ERK activation induced by VEGF (Fig. S1B). Interestingly, pSTAT3 Ser727 activation showed a slower activation pattern in contrast to the Tyr705 kinetics by peaking later at approximately 15 min (Fig. S1B). This signaling kinetics aligned with the observed wound-closure dynamic in OSM- versus VEGF-stimulated HUVECs. In summary, OSM activated multiple signaling pathways, whereas CNTF+R showed STAT3 specificity, with minor activation of STAT1 (Fig. 2C).

OSM+VEGF and CNTF+R+VEGF induce a transcriptomic shift with many similarities but also distinct differences

Based on the observed differences in the angiomodulatory potential as well as intracellular signaling patterns between OSM and CNTF+R in the presence of VEGF, we next examined whether these changes were associated with distinct gene expression profiles using RNA-sequencing (RNAseq) analysis. Principal component analysis (PCA) of whole-transcriptome-sequencing data revealed that OSM+VEGF and CNTF+R+VEGF led to transcriptomic profiles that were clearly separated from those of the VEGF control group by the first principal component (PC1, Fig. 3A) while the second principal component separated biological replicates within the same group (PC2, Fig. 3A). In comparison to VEGF, only a small shift in PC1 was observed between OSM+VEGF and CNTF+R+VEGF, suggesting that the transcriptomes of OSM+VEGF and CNTF+R+VEGF share many similarities and are distinct from those of VEGF, but are also different from each other. Comparing OSM+VEGF to the VEGF control group, 1392 differentially expressed genes (DEGs) were upregulated and 706 were downregulated. Between CNTF+R+VEGF and the VEGF control group, 1083 DEGs were upregulated and 431 downregulated. In contrast, only 92 genes were differentially upregulated and 35 differentially downregulated for OSM+VEGF in comparison to CNTF+R+VEGF (Fig. 3B). To identify genes responsible for the OSM-associated pro-angiogenic effect, we compared the transcriptomes of OSM+VEGF and CNTF+R+VEGF as the angiogenic differences would be reflected in them. A Gene Ontology (GO) term enrichment analysis of OSM+VEGF compared to CNTF+R+VEGF for biological processes identified ‘inflammatory response’, ‘response to cytokine’ and ‘cell migration’ as part of the ten most enriched terms for OSM+VEGF (Fig. 3C). A GO term enrichment analysis for molecular functions identified ‘cytokine receptor binding’, ‘growth factor binding’ and ‘growth factor receptor binding’ as some of the top enriched terms. Besides these, GO term clusters associated with immunological processes were enriched, and this enrichment was also measured in an enrichment analysis using the Reactome database, which resulted in

Journal of Cell Science (2023) 136, jcs260182. doi:10.1242/jcs.260182

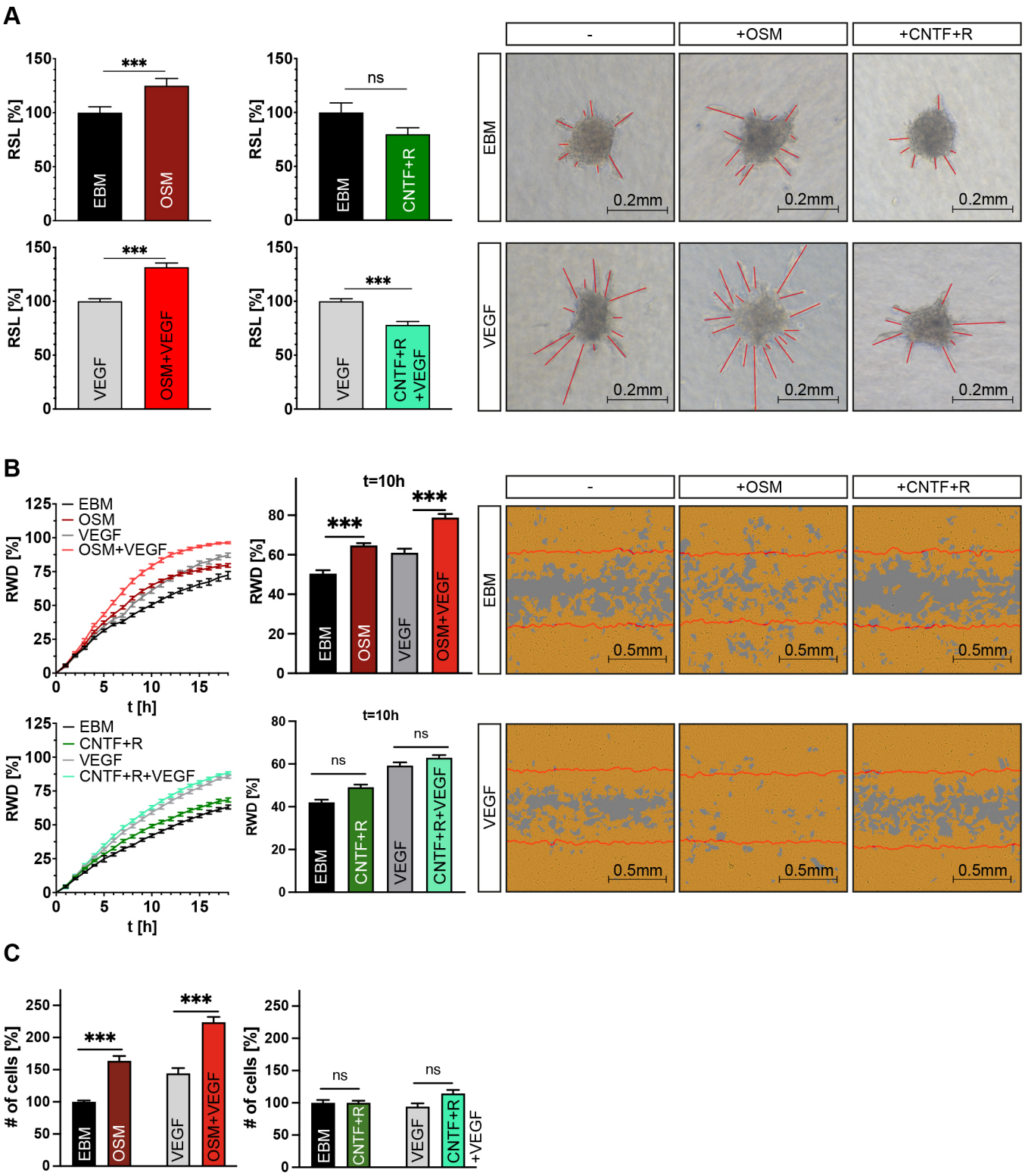

Fig. 1. OSM shows pro-angiogenic potential by activation of a broader range of signaling pathways in contrast to the anti-angiogenic CNTF+R. (A) Relative sprouting length (RSL, left) of HUVECs stimulated by endothelial basal medium (EBM) as a negative control, OSM and CNTF+R, with or without VEGF measured in the spheroid sprouting assay (right, red lines indicated sprouts). *n*=3–5 independent experiments with 12–20 spheroids per group and experiment. A Mann–Whitney *U*-test was used for statical analysis. (B) Relative wound density (RWD, left and middle) was measured over 18 h to determine the migratory effect of EBM, OSM, CNTF+R or VEGF on HUVECs in the scratch-wound assay (right, red lines indicate original wound edge at *t*=0 h). *n*=3 independent experiments each including six to eight technical replicates. A Kruskal–Wallis Test adjusted for multiple testing was used to determine significance 10 h after the start of the experiment. (C) Proliferation assay of HUVECs stimulated by specific cytokine treatment for 3 days. *n*=3 independent experiments with eight technical replicates each. A Kruskal–Wallis Test adjusted for multiple testing was used to determine significance. Data show the mean±s.e.m. ns, not significant; ***P<0.001.

Journal of Cell Science (2023) 136, jcs260182. doi:10.1242/jcs.260182

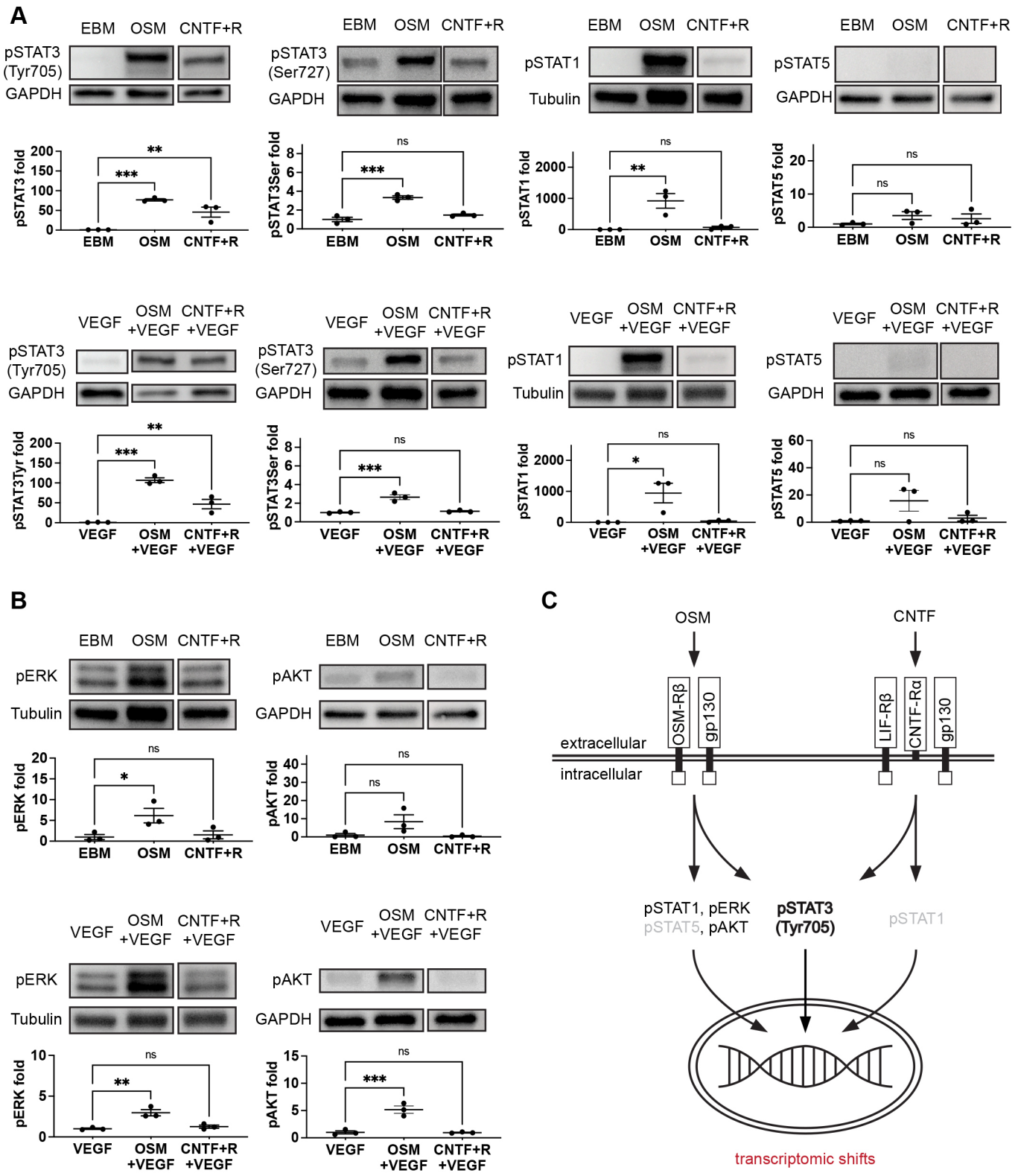

Fig. 2. OSM activates multiple other pathways beyond STAT3 signaling in contrast to CNTF+R. (A) Western blot analysis of HUVECs stimulated by EBM or cytokines for activation of STAT-related pathways. Protein lysates were collected after 15 min of stimulation, except for the pSTAT3 Ser727 blots, for which cells were incubated for 30 min. Statistical significance was calculated by one-way ANOVA adjusted for multiple testing with the two-stage step-up method of Benjamini, Krieger and Yekutieli. (B) Western blot analysis of HUVECs stimulated by EBM or cytokines for activation of the ERK und AKT pathways. Protein lysates were collected after 15 min of stimulation. Statistical significance was calculated by an ordinary one-way ANOVA adjusted for multiple testing with the two-stage step-up method of Benjamini, Krieger and Yekutieli. Data show the mean±s.e.m. ns, not significant; *P<0.05; **P<0.01; ***P<0.001. (C) Graphical summary of the activated pathways by OSM or CNTF+R as measured in the signaling analysis.

Journal of Cell Science (2023) 136, jcs260182. doi:10.1242/jcs.260182

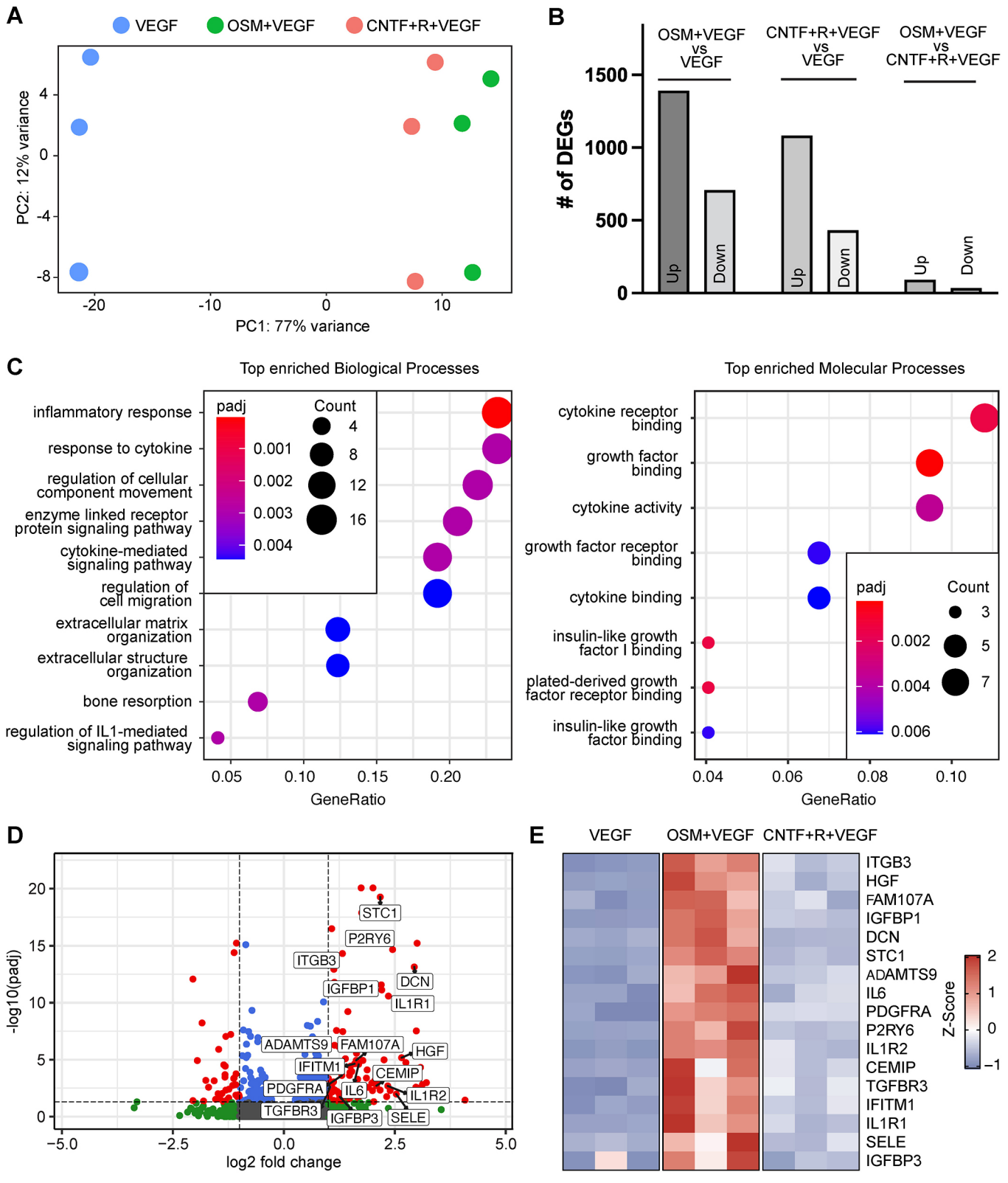

Fig. 3. See next page for legend.

enriched interleukin signaling clusters for OSM+VEGF-treated samples (Fig. S2). Most of the DEGs annotated to the GO terms 'cell migration', 'cytokine receptor binding', 'growth factor binding' and 'growth factor receptor binding' showed strong fold changes and were highly significant for OSM+VEGF (Fig. 3D). Gene-expression changes were consistent among biological replicates within the groups (Fig. 3E). Thus, the sequencing analysis suggests a conceivable role of the transcriptomic shifts inducing the observed angiogenic phenotype between the OSM+VEGF- and CNTF+R+VGEF-treated samples.

Journal of Cell Science

Fig. 3. The diverse angiomodulatory effect of OSM and CNTF+R on HUVECs corresponds to a distinct transcriptomic shift. (A) PCA of the HUVEC transcriptome following treatment with VEGF, VEGF+OSM or CNTF+R+VEGF for 24 h. (B) Bar graph visualizing the amount of DEGs measured for each condition. Up, upregulated DEGs; Down, downregulated DEGs. (C) Gene Ontology (GO) enrichment analysis of DEGs enriched for HUVECs treated with OSM+VEGF in contrast to CNTF+R+VEGF. The ten most significant GO terms according to the adjusted *P*-value (P_{adj}) are shown and ranked based on their share of the total number of DEGs (GeneRatio). Diagrams show terms enriched for OSM+VEGF and therefore depleted for CNTF+R+VEGF. The number of DEGs and the total number of genes for each GO term can be found in Tables S3 and S4. (D) Volcano plot of all genes with at least one count in both samples of HUVECs treated with OSM+VEGF or CNTF+R+VEGF. Genes defined as upregulated DEGs after OSM+VEGF treatment are marked in red. Genes which were not considered differentially expressed due to an absolute $\log_2$(fold change)<1 even though P_{adj}<0.05 are colored blue. Features with a $\log_2$(fold change)>1 but P_{adj}>0.05 are marked green. Genes annotated with the GO terms 'regulation of cell migration' (GO: 0030334), 'growth factor binding' (GO:0019838) or 'growth factor receptor binding' (GO:0070851) are labeled. (E) Heatmap of the Z-score of all labeled genes in D, visualizing the three replicates of each condition.

STAT3 knockdown enhances the pro-angiogenic potential of OSM and inverts the anti-angiogenic potential of CNTF+R on HUVECs

Having established significant differences in angiogenic cell behavior in response to OSM or to CNTF, we next assessed how the shared STAT3 pathway contributes to these phenotypes. We established a STAT3 knockdown protocol using siRNA, which resulted in a potent knockdown persisting for up to 96 h after transfection (Fig. S3A). In the spheroid-sprouting assay, STAT3 knockdown abrogated the basal sprouting rate in the EBM group and decreased VEGF-induced sprouting by 39% compared to cells transfected with control siRNA (Fig. 4A). In contrast, STAT3 knockdown led to the opposite effect in OSM+VEGF-stimulated HUVECs, characterized by a 2.06-fold increase in sprouting compared to the respective control siRNA-transfected cells and a 4.7-fold increase compared to STAT3 knockdown cells treated with VEGF alone.

STAT3 knockdown in HUVECs not only abolished the ability of CNTF+R to reduce VEGF-induced sprouting significantly, it also increased endothelial sprouting in the CNTF+R+VEGF group compared to the VEGF group by 1.78-fold. HUVECs transfected with control siRNA and CNTF+R+VEGF treatment still reduced sprouting by 40.8% (Fig. 4A). Comparing CNTF+R+VEGF-treated HUVECs with or without STAT3 knockdown, only a small difference was measurable, despite the massive decrease in sprouting caused by the STAT3 knockdown in samples treated only with VEGF (Fig. 4A).

Similar changes in response to STAT3 knockdown could be observed in the scratch-wound assay. STAT3 knockdown reduced the wound-closing kinetics of HUVECs in the EBM group by 27.6% and in the VEGF-treated group by 32.3% compared to the respective control siRNA-treated cells after 14 h (Fig. 4B). Stimulation with OSM in STAT3 knockdown cells led to a strong increase by a 3.258-fold change compared to EBM-stimulated STAT3 knockdown cells (Fig. 4B). Comparable effects were observed in the presence of VEGF: co-stimulation with OSM+VEGF following STAT3 knockdown increased migration by 2.05-fold compared to VEGF after 14 h (Fig. 4B). OSM treatment in control siRNA-transfected cells still led to a 1.51-fold increase in wound-closing kinetics and, upon co-stimulation with VEGF, it led to a 1.16-fold increase in wound-closing kinetics. Surprisingly, STAT3 knockdown significantly decreased OSM+VEGF-induced cell proliferation (Fig. S4), whereas VEGF-induced proliferation was also significantly reduced, suggesting that the observed phenotype in the spheroid-sprouting and migration assays are not based on enhanced proliferation but rather on migration and hypertrophy.

To ensure that the observed knockdown results were not skewed by siRNA off-target effects, we repeated selected knockdown experiments with a second STAT3 siRNA of a different sequence. STAT3 siRNA #2 resulted in a long-lasting, efficient knockdown (Fig. S3B). The spheroid-sprouting assay showed comparable changes in endothelial cell sprouting following STAT3 knockdown and OSM stimulation compared to STAT3 siRNA #1 (Fig. S3C), thus validating our STAT3 knockdown data. The same tendencies for the second STAT3 siRNA were also measurable in a screening experiment for CNTF+R using the second STAT3 siRNA (Fig. S3D).

To further validate the specificity of the observed STAT3-dependent phenotype, we established a STAT1 knockdown using siRNA (Fig. S3E) and repeated the sprouting assay. Similar to the STAT3 knockdown, the STAT1 knockdown decreased the basal sprouting rate in every group (average decrease of 46.3%, Fig. S3F). The increase in sprouting in the OSM treatment group was abolished following STAT1 knockdown. In contrast to the STAT3 knockdown that led to a significant increase in sprouting, OSM+VEGF only induced a weak increase in sprouting by 18.1% compared to VEGF following STAT1 knockdown (Fig. S3F). These data further validate the specificity of the observed STAT3 knockdown data.

The increase in the pro-angiogenic effect of OSM following STAT3 knockdown correlates with a shift in the balance of intracellular signaling pathways

To better understand the molecular mechanisms behind the enhanced pro-angiogenic potential of OSM following STAT3 knockdown, we next performed RNAseq analysis of HUVECs co-stimulated with OSM and VEGF following STAT3 knockdown (OMS+VEGF STAT3 siRNA) compared to control siRNA-transfected cells (OSM+VEGF control siRNA). In the OSM+VEGF STAT3 siRNA group, 2410 DEGs were detected. GO enrichment analysis of all DEGs revealed many immunological terms, in line with the well-characterized role of STAT3 in inflammation. Interestingly, multiple GO terms associated with the regulation of the MAPK pathways and interferon-γ signaling pathway, which is closely connected to the STAT1 signaling pathway and known for its role in angiogenesis, were enriched as well (Fig. 5A). A pro-migrative transcriptome was also triggered by STAT3 knockdown in OSM+VEGF-treated HUVECs, indicated by the enrichment of the GO term 'positive regulation of cell migration'. Although STAT3 knockdown cells showed a depletion of genes associated with 'negative regulation of growth' (Fig. 5A), as indicated by an enrichment in GO terms in the RNAseq data from the control siRNA samples treated with OSM+VEGF, this did not translate in a functional alteration as described earlier (Fig. S4). Most of the DEGs annotated to GO terms associated with MAPK, cell migration and interferon-γ activity presented good clustering on a sample-to-sample level (Fig. 5B). Three out of the five most strongly expressed upregulated DEGs (Fig. 5C, marked in red) in OSM+VEGF-treated STAT3 knockdown cells were part of the GO 'angiogenesis' cluster (GO:0001525), which was not among the top 15 regulated GO terms shown in Fig. 5A, but was significantly enriched in knockdown cells. Gene set enrichment analysis (GSEA) confirmed that overall, genes associated with the GO term angiogenesis were significantly enriched in the

Journal of Cell Science (2023) 136, jcs260182. doi:10.1242/jcs.260182

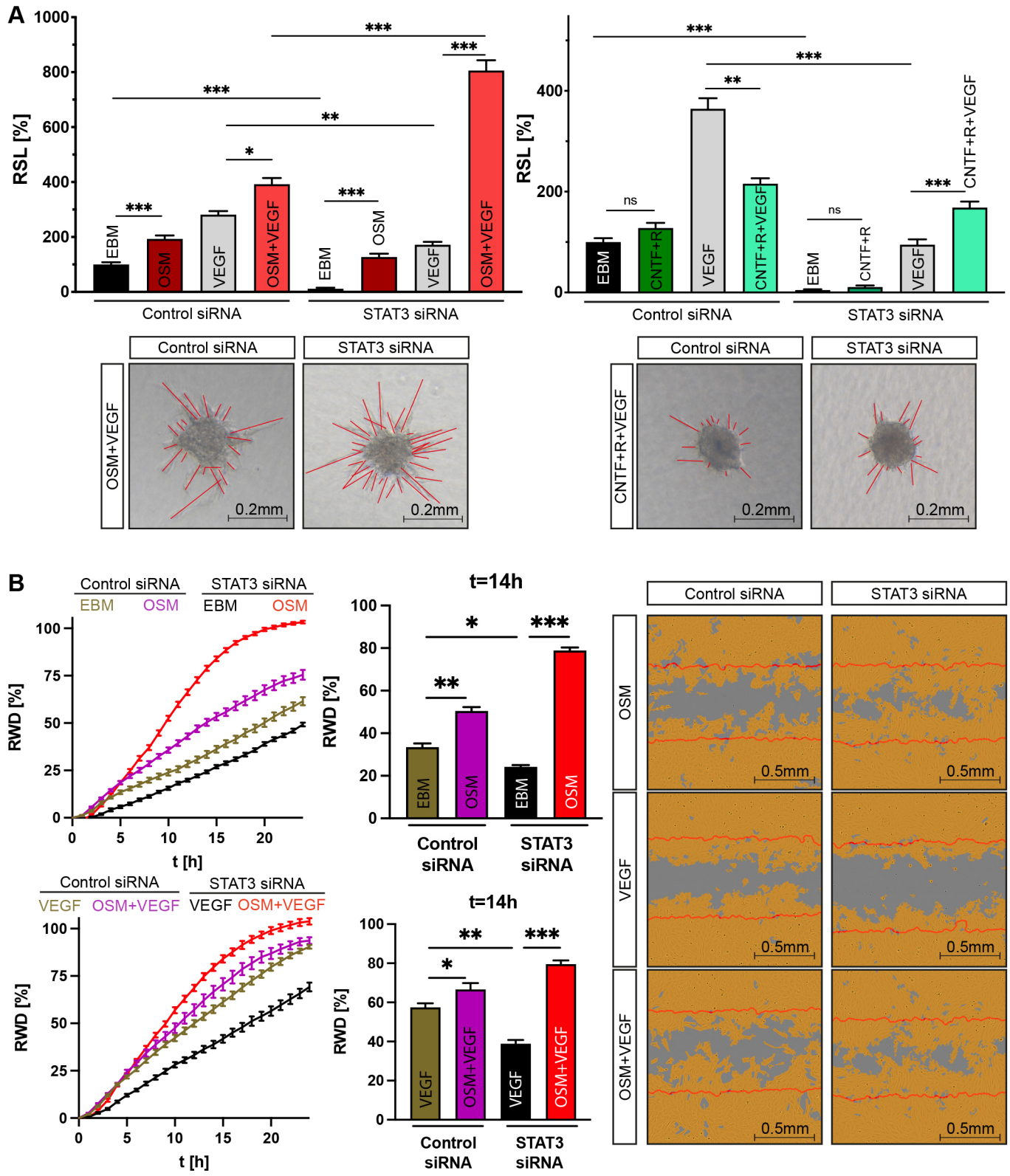

Fig. 4. STAT3 knockdown enhances the pro-angiogenic effect of OSM and abolishes the anti-angiogenic influence of CNTF on HUVECs. (A) Endothelial sprouting of HUVECs in response to the EBM control, OSM, CNTF+R, VEGF or a combination of the above was measured by the relative sprouting length (RSL, top) in the spheroid sprouting assay (bottom) following STAT3 knockdown and compared to controls treated with control siRNA. Data are representative of three independent experiments each consisting of 12–20 spheroids per group and experiment. Statistical testing was conducted by a Kruskal–Wallis test adjusted for multiple testing. (B) Relative wound density (RWD, left and middle) of HUVECs in response to stimulation with EBM, OSM, VEGF or a combination was determined in the scratch-wound assay of HUVECs transfected with STAT3 siRNA or control siRNA. *n*=3 individual experiments which include six to eight technical replicates each. A Kruskal–Wallis test adjusted for multiple testing was used to determine significance 14 h after stimulation. Data show the mean±s.e.m. ns, not significant; **P*<0.05; ***P*<0.01; ****P*<0.001.

Journal of Cell Science (2023) 136, jcs260182. doi:10.1242/jcs.260182

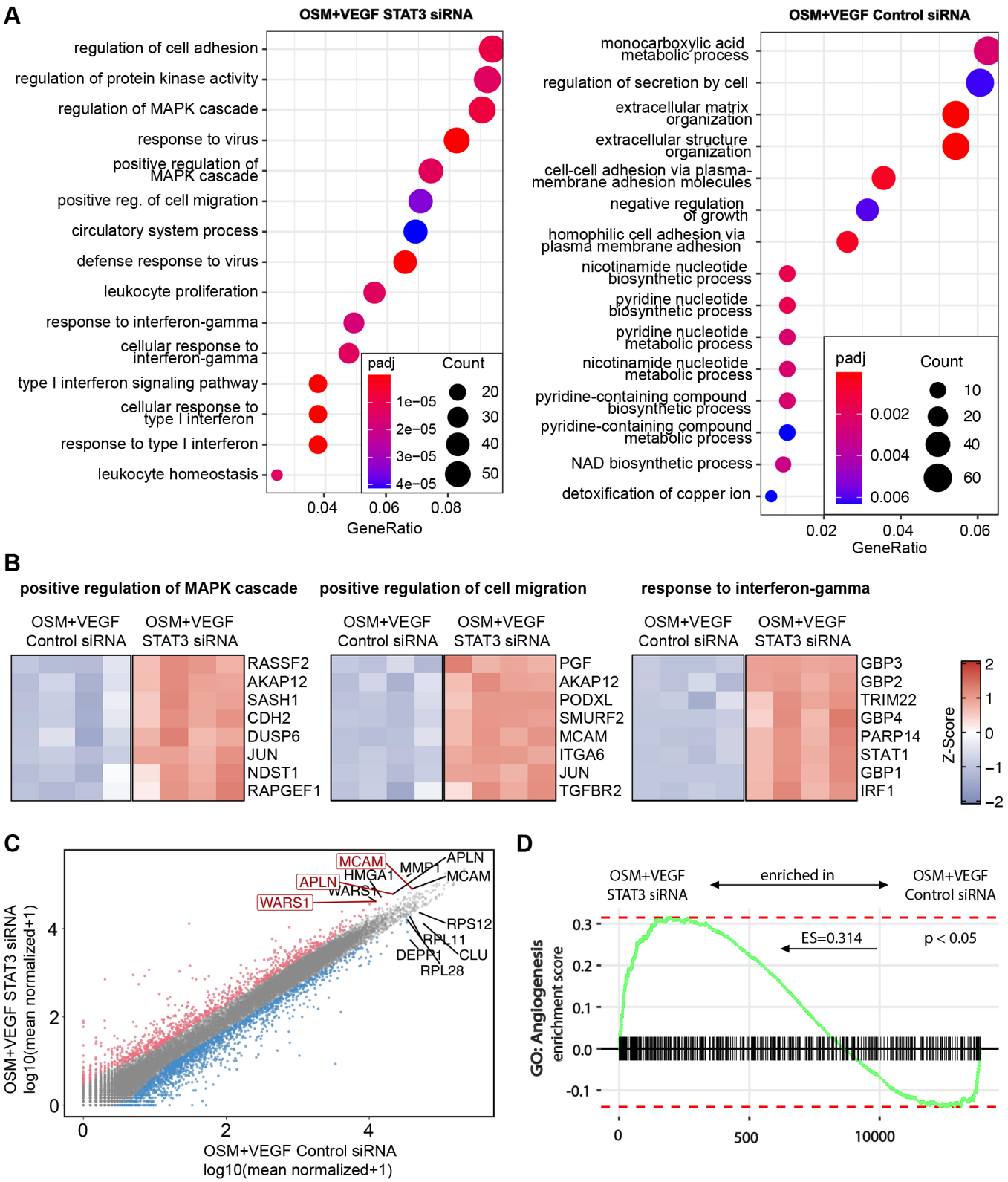

Fig. 5. See next page for legend.

OSM+VEGF STAT3 siRNA group (Fig. 5D). Taken together, these results strongly suggest that the enhanced pro-angiogenic effect of OSM in the absence of STAT3 is related to the upregulation of STAT1- and ERK-dependent genes associated with cell proliferation and angiogenesis.

To understand whether a suspected compensatory upregulation of STAT1 and ERK signaling in response to STAT3 knockdown and OSM+VEGF treatment was specific to OSM, we also analyzed the transcriptomic profile of HUVECs treated with CNTF+R+VEGF following STAT3 knockdown (CNTF+R+VEGF STAT3 siRNA)

Journal of Cell Science (2023) 136, jcs260182. doi:10.1242/jcs.260182

Fig. 5. STAT3 knockdown in HUVECs induces a transcriptomic shift towards a dysregulated state of proliferation, migration and vascular development in response to OSM treatment, including upregulation of ERK- and STAT1-associated signaling pathways on the RNA level. (A) GO term enrichment analysis of DEGs enriched for HUVECs treated with OSM+VEGF following STAT3 knockdown (STAT3 siRNA) or treatment with control siRNA. The 15 statistically most significant GO terms according to the adjusted *P*-value (P_{adj}) are shown and ranked by their share of the total number of DEGs (GeneRatio). The diagrams show the enriched terms for the labeled conditions. The number of DEGs and the total number of genes for the GO terms can be found in in Tables S5 and S6. (B) Heatmaps of the eight most expressed DEGs tagged with GO terms associated with positive regulation of MAPK signaling (GO:0043410), response to the interferon-γ pathway (GO:0034341) and positive regulation of cell migration (GO:0030335) visualized by the Z-score in each replicate. (C) Scatterplot of all genes with at least one count in HUVECs treated with OSM+VEGF following STAT3 knockdown compared to the control siRNA group. Genes defined as upregulated DEGs in response to OSM+VEGF treatment following STAT3 knockdown are marked in red and differentially downregulated genes are marked in blue. The top five upregulated and downregulated DEGs according to their absolute expression are labeled. Genes which are related to the GO term 'angiogenesis' (GO:0001525) are highlighted. (D) GSEA for the GO term 'angiogenesis' in HUVECs treated with OSM+VEGF following STAT3 knockdown.

as well as with VEGF following STAT3 knockdown (VEGF STAT3 siRNA). Comparing CNTF+R+VEGF-treated knockdown and control cells, multiple enriched GO terms associated with interferon-γ signaling, but not MAPK signaling, were identified (Fig. S5A; Tables S7 and S8). These data align with initial analyses indicating that CNTF+R, in contrast to OSM, activated STAT3 and STAT1 signaling but not ERK signaling (Fig. 2B). A scatter plot of the data again illustrated many highly expressed DEGs annotated for GO angiogenesis including *WARS1* and *APLN* (Fig. S5B). GSEA was also significantly enriched for the GO term 'angiogenesis' (Fig. S5C). In contrast, VEGF-stimulated HUVECs with or without STAT3 knockdown retrieved only six significantly enriched biological processes in the GO enrichment analysis (Fig. S6A,B; Tables S9 and S10). Again, this aligns with the observation that VEGF does not induce STAT3 signaling in HUVECs.

The observed transcriptomic shifts in the OSM+VEGF- as well as the CNTF+R+VEGF-treated groups following STAT3 knockdown point towards compensatory upregulation of STAT1 signaling and, in the case of OSM+VEGF, ERK signaling. We therefore re-evaluated the activity of intracellular signaling pathways following STAT3 knockdown with cytokine stimulation on protein level using western blotting. Following STAT3 knockdown and 5 min of OSM+VEGF stimulation, there was no enhanced activation of pSTAT1, pSTAT5, pAKT and pERK, whereas the pSTAT3 signal was clearly diminished (Fig. 6A). However, time-course experiments that screened for differences in pSTAT1 activity over 24 h revealed that STAT3 knockdown cells showed a clearly prolonged pSTAT1 activity after 6 h and 24 h in response to OSM+VEGF treatment (Fig. 6B).

In summary, these data suggest that the extent of the pro-angiogenic effect of OSM is tightly regulated by the balance of intracellular signaling activity. Blocking STAT3 enhances cell migration and sprouting, which is reflected by significantly upregulated genes associated with cell migration and compensatory signaling pathways, including ERK and AKT, which in turn have been associated with a pro-angiogenic effect in previous studies (Fig. 6C) (Zhang et al., 2019; Jiang and Liu, 2008).

OSM shifts HUVECs to an active metabolic state by increasing mitochondrial performance

Examining alternative phosphorylation sites of STAT3 in response to OSM and CNTF, we observed that only OSM promoted phosphorylation of STAT3 not only at Tyr705, but also at Ser727 (pSTAT3 Ser727) (Fig. 2A). pSTAT3 Ser727 has been described to enhance the transcriptomic impact of STAT3 and it modulates mitochondrial function to consequently change the metabolic rate of cells (Gough et al., 2009, 2014; Wegrzyn et al., 2009; Balic et al., 2020). We hypothesized that OSM increases the mitochondrial function of HUVECs by phosphorylation of STAT3 at the Ser727 site and thus provide the energy and metabolites necessary for the enhanced angiogenic process. Using OSM-stimulated bovine aorta endothelial cells (BAECs) transfected with plasmids expressing STAT3 tagged with a fluorescent protein, co-localization of STAT3 and stained mitochondria was evident (Fig. 7A). Unstimulated cells did not yield this result (Fig. 7A). Extracellular flux analysis of HUVECs pretreated with cytokines overnight for 15 h provided a precise readout for further functional metabolic switches. Pretreatment with OSM or OSM+VEGF led to an increase in basal respiration, ATP production and maximal respiration in comparison to cells treated only with EBM (Fig. 7B,C). VEGF and CNTF+R did not significantly alter any of these functions.

To screen for potential molecular reasons that might explain the enhanced metabolic activity of HUVECs in response to OSM, we next studied the levels of mitochondrial respiratory chain complexes. Western blot analysis of all important complexes in the respiratory chain did not show any changes at the protein level (Fig. 8A) or at the RNA level by RNASeq (Fig. S7). The major production of superoxide was also not changed compared to control groups (Fig. 8B). Although OSM induced mitochondrial activity consistently, the underlying molecular mechanisms remain to be elucidated.

OSM treatment enhances glycolysis

While measuring mitochondrial activity by extracellular flux analysis, OSM was also found to enhance glycolytic activity in vascular endothelial cells (Fig. 8C,D). This observation might be of particular relevance in the context of angiogenesis as glycolysis is believed to represent the main energy provider in hypoxia-driven angiogenic processes (Potente and Carmeliet, 2017). Quantification of the extracellular acidification rate (ECAR) results revealed that baseline glycolytic activity was only significantly enhanced in the VEGF+OSM group compared to the VEGF group, whereas maximal glycolytic capacity was significantly increased in cells treated with OSM or OSM+VEGF compared to the respective controls (Fig. 8C,D). In contrast, CNTF+R stimulation did not result in similar changes (Fig. 8C,D).

Taken together, the pro-angiogenic potential of OSM appears to be rooted in the activation of strong proliferative stimuli on a transcriptomic as well as metabolic level, affecting mitochondrial respiration as well as glycolysis.

DISCUSSION

In this study, we examined the angiomodulatory effects and underlying molecular changes of the IL-6 family members and STAT3 activators OSM and CNTF to better characterize the role of STAT3 signaling in angiogenesis. Using *in vitro* angiogenesis assays, we confirmed the previously described pro-angiogenic

Journal of Cell Science (2023) 136, jcs260182. doi:10.1242/jcs.260182

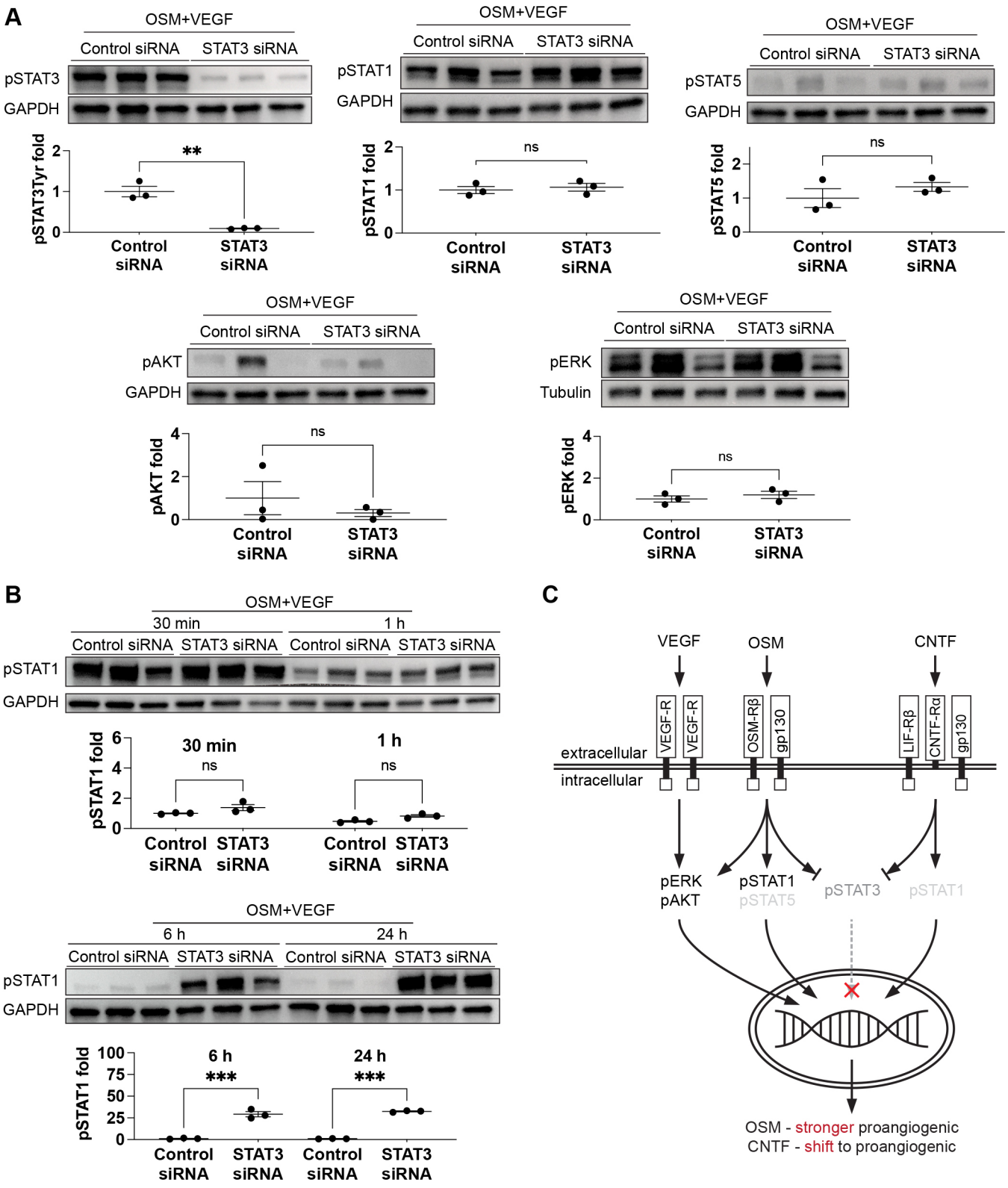

Fig. 6. Compensatory changes of intracellular signaling pathways in response to STAT3 knockdown and OSM+VEGF treatment. (A) Comparison of intracellular signaling patterns in HUVECs after successful STAT3 knockdown and treatment with different cytokines for 5 min using western blotting. *n*=3 independent experiments; two-tailed unpaired Student's *t*-test. (B) Western blot analysis for pSTAT1 at 30 min, 1 h, 6 h and 24 h in OSM+VEGF-treated HUVECs with or without STAT3 knockdown. *n*=3 independent experiments; two-tailed unpaired Student's *t*-test. Data show the mean±s.e.m. ns, not significant; ***P*<0.01; ****P*<0.001. (C) Graphical summary of the altered signaling patterns by OSM and CNTF+R and how the angiogenic phenotype changed due to knockdown.

Journal of Cell Science (2023) 136, jcs260182. doi:10.1242/jcs.260182

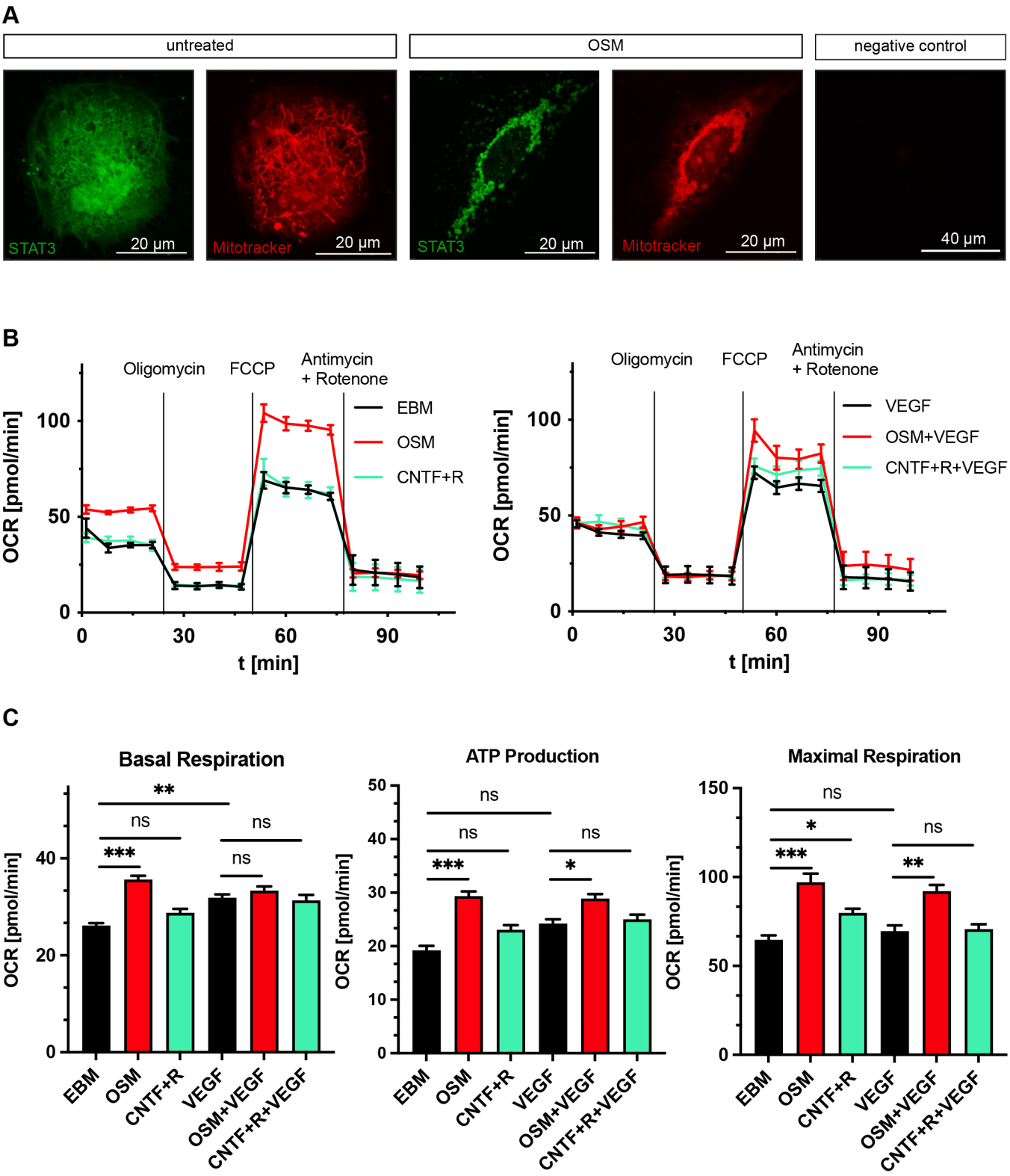

Fig. 7. STAT3 accumulates in mitochondria after OSM treatment and increases mitochondrial activity. (A) Immunocytochemical analysis of BAECs transfected with Venus-WTSTAT3 plasmids. BAECs were stimulated with OSM or negative control for 30 min and stained with MitoTracker. The negative controls were BAECs transfected with no plasmid and no incubation with MitoTracker. (B) Representative graphs of the oxygen consumption rate (OCR) of HUVECs pretreated overnight with different cytokines or EBM using Seahorse XF Cell Mito Stress Test. Each graph includes six to eight technical replicates. Data were normalized to the measured cell count in each well. (C) Normalized quantification of the Seahorse XF Cell Mito Stress Test results from HUVECs pretreated with cytokines or EBM overnight. Data are representative of three independent experiments including six to eight technical replicates each. A Kruskal–Wallis adjusted for multiple testing was used for statistical analysis. Data show the mean±s.e.m. ns, not significant; *P<0.05; **P<0.01; ***P<0.001.

Journal of Cell Science (2023) 136, jcs260182. doi:10.1242/jcs.260182

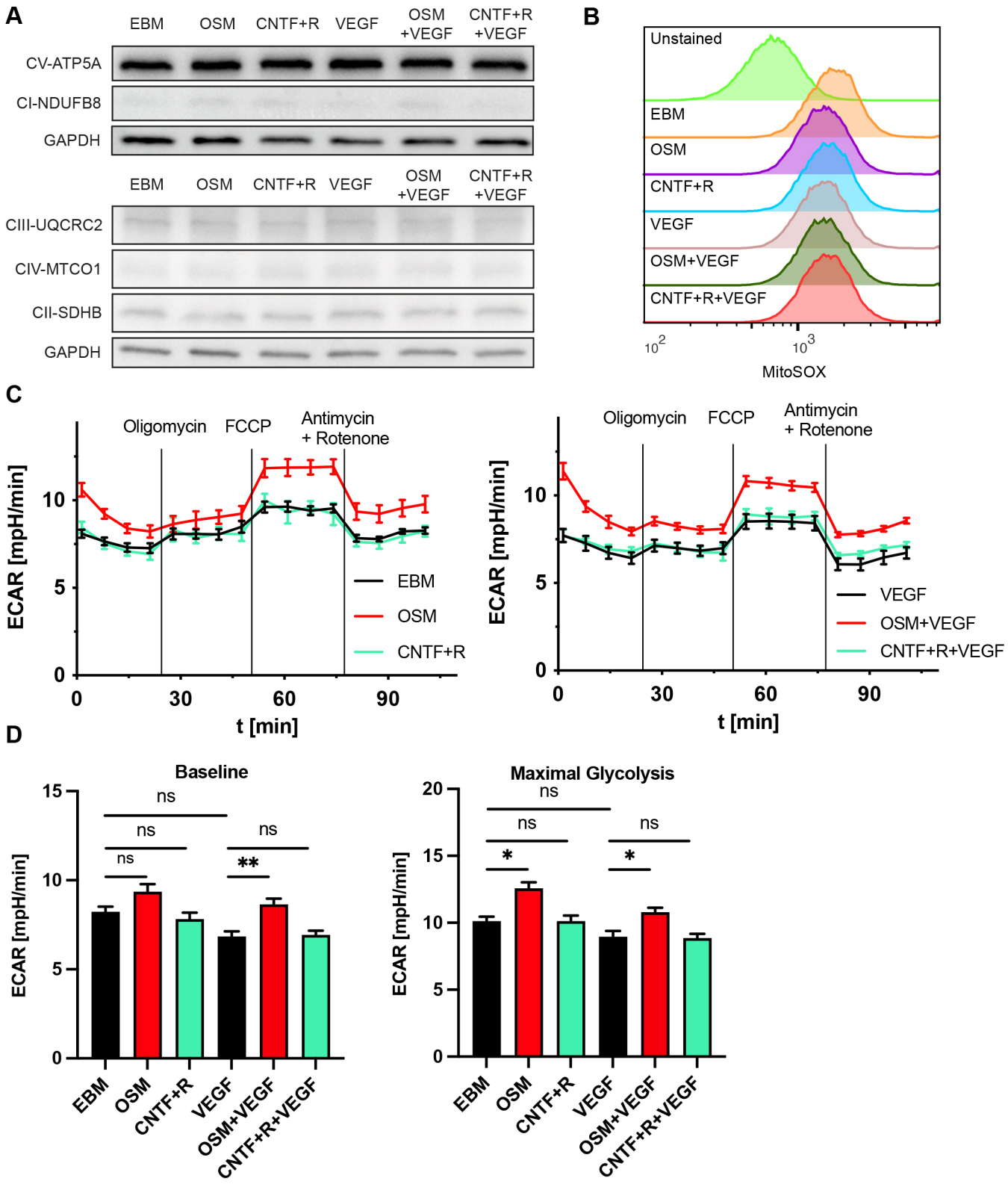

Fig. 8. Analysis of metabolic changes induced by OSM or CNTF+R treatment in HUVECs. (A) Western blot analysis of the expression of mitochondrial complex I (CI-NDUFB8), complex II (CII-SDHB), complex III (CIII-UQCRC2), complex IV (CIV-MTCO1) and complex V (CV-ATP5A) after overnight treatment with cytokines or EBM. (B) Exemplary flow cytometry measurements for the production of ROS after pretreatment of HUVECS with cytokines or EBM overnight using the MitoSOX assay. (C) Representative graphs of the extracellular acidification rate (ECAR) of HUVECs pretreated overnight with EBM or different cytokines using the Seahorse XF Cell Mito Stress Test. Each graph includes six to eight technical replicates. Data are normalized to the measured cell count in each well. (D) Normalized quantification of the glycolytic activity of HUVECs pretreated with EBM or cytokines overnight. *n*=3 independent experiments including six to eight technical replicates each. A Kruskal–Wallis test was used for statistical analysis and adjusted for multiple testing. Data show the mean±s.e.m. ns, not significant; **P*<0.05; ***P*<0.01; ****P*<0.001.

effect of OSM (Vasse et al., 1999) and anti-angiogenic effect of CNTF (Bucher et al., 2016, 2020) on vascular endothelial cells in standardized experimental settings (Fig. 1). Next, we elucidated the underlying mechanisms responsible for the inverse phenotype by characterizing intracellular signaling activity beyond STAT3 signaling (Fig. 2). STAT3 knockdown experiments and RNAseq analyses were used to further address the impact of STAT3 in the context of other pro-angiogenic signaling pathways (Figs 4–6).

At first, our results about the role of STAT3 signaling in vascular endothelial cells appear to contradictory: STAT3 knockdown decreased endothelial cell migration and sprouting in untreated or VEGF-stimulated cells, whereas STAT3 knockdown in IL-6 family cytokine-induced angiogenesis led to increased migration and sprouting (Fig. 4). Earlier studies on the role of STAT3 signaling in cell biology reveal that STAT3 modulates cellular functions on different levels depending on its subcellular localization and phosphorylation status (Avalle and Poli, 2018).

Our observation that STAT3 knockdown in unstimulated and VEGF-stimulated HUVECs significantly decreased endothelial cell migration and sprouting is in line with previously published data, which led to the common perception of STAT3 being a driver of angiogenesis (Jung et al., 2005; Johnson et al., 2018; Hu et al., 2019). Interestingly, both conditions (EBM as well as VEGF treatment) did not induce any baseline activation of the STAT3 signaling pathway, represented by phosphorylation of STAT3 (Fig. 2). The measured decrease of angiogenesis might be due to a cytoplasmatic function of STAT3 independent of its phosphorylation status. Teng et al. (2009) proposed an interaction of STAT3 with the cytoskeleton that negatively affects cell migration after STAT3 loss. Ng et al. (2006) provided evidence for the interaction of STAT3 and the microtubule network, showing that STAT3 knockdown led to microtubule disassembly, resulting in decreased endothelial capacity to migrate into a cell-free area *in vitro*. Our own immunohistochemical staining of the actin cytoskeleton by phalloidin suggested that STAT3 knockdown significantly reduced lamellipodium formation (data not shown), which is reported to be dependent on proper microtubule formation (Mikhailov and Gundersen, 1998). Furthermore, a role of unphosphorylated STAT3 as a transcription factor is also discussed in the literature (Timofeeva et al., 2012). This suggests that changes in expression levels of the downstream targets of unphosphorylated STAT3 could also be sufficient to induce shifts in phenotype owing to STAT3 knockdown. Although the idea of a protein–protein interaction of unphosphorylated STAT3 in the cytosol is still controversial, our own and previously published data suggest a more diverse role of STAT3 in cell biology beyond its role as a transcription factor in its phosphorylated form.

Starting from the observed decrease in endothelial cell migration and sprouting in STAT3 knockdown cells following control and VEGF treatment, it was intriguing to observe an increase in endothelial cell migration and sprouting in response to OSM+VEGF or CNTF+R+VEGF stimulation following STAT3 knockdown (Fig. 4). Treatment with OSM+VEGF or CNTF+R+VEGF led to phosphorylation of STAT3 as well as other signaling molecules, including ERK (Fig. 2), which was associated with distinct shifts in the transcriptomic profile (Fig. 3). Under the circumstance of STAT3 loss due to knockdown, other pathways in response to OSM+VEGF and CNTF+R+VEGF, such as pERK, remained active (Fig. 6). We therefore assume that pSTAT3 balances the influence of pro-angiogenic drivers like ERK or AKT on a transcriptomic level. Besides clustering of ERK-associated GO terms, RNAseq analysis of OSM+VEGF STAT3 siRNA cells showed enriched clusters of type I interferon and interferon-γ associated signaling (Fig. 5A). We assume that this is an indication for the increased impact of pSTAT1 on the transcriptome because type I interferon and interferon-γ use the STAT1 pathway as a second messenger (Jung et al., 2021). Owing to increased pSTAT1 impact on the transcriptome induced by STAT3 knockdown, both of those GO terms were enriched without any actual stimulation by type I interferons or interferon-γ. Western blot analysis revealing prolonged pSTAT1 activity over 24 h after STAT3 knockdown support this hypothesis (Fig. 6B). Normally, pSTAT1 activity is associated with an anti-angiogenic properties (Huang et al., 2002), which questions the role of the prolonged pSTAT1 activity in the increased pro-angiogenic drive of OSM+VEGF after STAT3 knockdown. We therefore assume that our data underline the important regulatory function of STAT3 on the activity of other signaling pathways that modulates their ability to change their capability of shifting the transcriptome, which in total dictates the behavior of the endothelial cell.

The complexity of STAT3 signaling is further increased due to the existence of multiple phosphorylation sites that modulate STAT3 activity in different subcellular compartments. Besides the Tyr705 phosphorylation site, STAT3 signaling can further be altered by phosphorylation at Ser727, which is reported to increase mitochondrial performance and oxidative phosphorylation activity (Gough et al., 2009, 2014; Wegrzyn et al., 2009; Balic et al., 2020). In contrast to CNTF, only OSM led to STAT3 Ser727 phosphorylation (Fig. 2A). Although vascular endothelial cells are known to mainly rely on glycolysis to fuel their need for ATP, they can also use mitochondrial oxidation under stress and mitochondria as a biosynthetic hub to produce metabolites necessary for angiogenesis (Potente and Carmeliet, 2017). The molecular mechanism behind the impact of pSTAT3 Ser727 on cell metabolism is still not fully understood. Current work suggests an interaction between STAT3 and respiratory complexes I and II to increase their activity, leading to membrane potential enhancement (Wegrzyn et al., 2009), and a regulatory function of STAT3 in the production of reactive oxygen species (Gough et al., 2009). Mitochondrial STAT3 is also recognized to change mitochondrial gene expression (Carbognin et al., 2016). The ability of OSM to increase mitochondrial performance and biogenesis while reducing apoptotic behavior has been reported in cardiomyocytes (Sun et al., 2015). Hanlon et al. (2019) recently described increased glycolysis in endothelial cells treated with OSM, but no improvement in mitochondrial performance was observed, whereas our data suggest an increase in mitochondrial respiration as well as glycolysis (Fig. 7B,C, Fig. 8C,D). In contrast to our setup, Hanlon et al. (2019) pretreated HUVECs for 3 h in comparison to our 15 h overnight incubation. The increase in oxidative phosphorylation might need more time to unfold, whereas the boost in glycolysis measured by Hanlon et al. (2019) represents a potentially immediate reaction. An instantaneously increased ECAR by an OSM injection to untreated cells in a Seahorse extracellular flux assay, which we also measured (data not shown), supports this hypothesis. However, we did not observe OSM-associated differences by screening for major changes in the expression levels of mitochondrial complexes or the production of reactive oxygen species induced by severe oxidative stress (Fig. 8A,B). The increased metabolic rate could be triggered by an unknown protein–protein interaction, which warrants further understanding of the link between OSM and metabolism, especially because pSTAT3 Ser727-induced metabolic switches were linked to disease progression (Zhang et al., 2013; Gough et al., 2014).

In summary, our study outlines the complex role of STAT3 signaling in vascular endothelial cells in response to cytokine treatment, which consequently results in pleiotropic angiogenic

Journal of Cell Science (2023) 136, jcs260182. doi:10.1242/jcs.260182

effects. The angiomodulatory effect of STAT3 appears to be dependent on the activity of other intracellular signaling pathways as well as its subcellular localization in the cytosol, mitochondria or nucleus. OSM and CNTF differ in their intracellular signaling patterns and their STAT3 specificity, which translates into unique transcriptomic profiles and metabolic activity. A profound knowledge of these fine differences is necessary to understand the contribution of STAT3 signaling to disease progression and to subsequently use STAT3 or STAT3-activating cytokines as therapeutic targets.

MATERIALS AND METHODS

HUVEC culture

HUVECs (pooled in EGM-2, C2519A, Lonza, Basel, Switzerland) were grown in endothelial cell growth medium (EGM, CC-3162, Lonza) and used for all *in vitro* experiments.

For protein and RNA analyses, cells were stimulated by cytokines (summarized in Table S1), which were diluted in endothelial cell growth basal medium 2 (EBM-2, CC-3156, Lonza) supplemented with 6% fetal bovine serum (FBS, S0615, Biochrom, Berlin, Germany). Cytokines and their concentrations can be found in Table S1. For protein analysis, cells were lysed after 5 min of cytokine stimulation using T-PER tissue protein extraction reagent (78510, Thermo Fisher Scientific) supplemented with phosphatase and proteinase-inhibitor (87786 und 78420, Thermo Fisher Scientific). For RNA sample generation, cells were lysed in QIAzol lysis reagent (79306, QIAGEN, Hilden, Germany) 24 h after stimulation.

Transfection

HUVECs were transfected using a loading solution of Opti-MEM (31985062, Thermo Fisher Scientific) containing 0.4% Lipofectamine RNAiMAX (137780309, Thermo Fisher Scientific) and 15 nM STAT3 Stealth siRNA (1299001, siRNA ID: VHS40491, Thermo Fisher Scientific), 120 nM STAT1 Stealth siRNA (1299001, siRNA ID: VHS40871, Thermo Fisher Scientific) or control siRNA (Stealth RNAi siRNA negative control, Med GC, 12935300, Thermo Fisher Scientific) for 6 h. After 6 h, wells were filled up to 2 ml using EGM. Cells were used for assays 48 h after transfection. On-target accuracy of the knockdown was evaluated by comparing effects of a second STAT3 Stealth siRNA (1299001, siRNA ID: VHS40497, Thermo Fisher Scientific) with a completely different sequence.

SDS PAGE and western blotting

Protein samples were prepared for electrophoresis by denaturation using 75% sample, 22.5% Laemmli Buffer (4× Laemmli Sample Buffer, 1610747, Bio-Rad) and 2.5% 2-mercaptoethanol (M3148, Sigma-Aldrich). Samples were separated by SDS-PAGE and then transferred to a Immobilon-P PVDF Membrane (IPVH00010, Millipore). Following a blocking step with 3% bovine serum albumin (BSA, Albumin, Rind, Fraction V, Protease-free, 11926.03, Serva, Heidelberg, Germany) for 30 min, membranes were stained with primary antibodies overnight at 4°C. Staining for GAPDH and secondary antibodies was conducted on the following day for 1 h. All antibodies and their respective dilutions can be found in Table S2. A Fusion FX system (Vilber, Collégien, France) detected the signal using the ECL Prime Western Blotting System (RPN2232, GE Healthcare). Figures show representative western blot results of three independent experiments. Where applicable, western blots were semiquantitatively analyzed by using ImageJ Fiji and its gel analyzer platform. Data were normalized by using GAPDH expression levels for each lane, which served as protein loading control. The relative fold change of protein expression was finally calculated as a percentage by normalizing data to the specific control group. Uncut blots can be found in Figs S8–S12.

Spheroid sprouting assay

Spheroids formed in hanging drops of EGM containing 0.25% methylcellulose (M0512, Sigma-Aldrich) overnight were seeded in 0.5 ml of a collagen matrix consisting of 50% rat tail collagen (354236, Corning) and 48% EBM containing 0.25% methylcellulose and 2% FBS. Collagen was titrated to a physiological pH by using sodium hydroxide (P031.2, Roth, Karlsruhe, Germany) and buffered with 1 µl of a 1 M HEPES buffer (P05-01100, PAN Biotech, Aidenbach, Germany) After solidifying the gel for 30 min, the wells were layered with 100 µl EBM containing cytokines to match the desired final concentration. After incubation for 1 day, images of spheroids were taken using an inverse microscope (Zeiss Axio Vert A1, Jena, Germany) and the imaging software 'ProgPres CapturePro 2.10.0.1' (Jenoptik Optical Systems, Jena, Germany). Quantification of all sprouts in each image took place using the measuring tool of ImageJ Fiji. The relative sprouting length (RSL) per spheroid was used as a final readout by calculating the average cumulative sprouting length per spheroid normalized to the respective control from the same experiment.

Scratch-wound assay

The migratory potential of HUVECs was measured by a standard scratch assay. Approximately 20,000 HUVECs per well were seeded in EGM in IncuCyte ImageLock 96-well plates (4379, Sartorius, Göttingen, Germany) and starved overnight using EBM supplemented with 2% FBS and antibiotics. On the following day, the scratch was created using the IncuCyte WoundMaker (IncuCyte Cell Migration Kit, 4493, Sartorius) and wells were imaged every hour for 18–24 h by the IncuCyte S3 Live-Cell Analysis System (4647, Sartorius). For analysis, the integrated IncuCyte software (Integrated Cell Migration analysis module, 9600-00-12, Sartorius) primed for HUVECs automatically detected cells and cell migration. The relative wound density (RWD) was calculated automatically by the software and used as a final readout by dividing the confluence inside the originally scratched area by the confluence outside this area.

Proliferation assay

Approximately 3000 HUVECs were seeded into 96-well plates in EBM with 6% FBS. After 3 h, cells were stimulated by cytokines diluted in EBM supplemented with 6% FBS for a total of 72 h, with a medium change containing fresh cytokines every 24 h. Cell number was determined by following the CyQUANT Cell Proliferation Assay protocol (C7026, Thermo Fisher Scientific). The readout was normalized to the specific control group during data analysis.

Extracellular flux analysis

Metabolic shifts were assessed using extracellular flux analysis by a Seahorse XFe96 Analyzer (Agilent Technologies), measuring the oxygen consumption rate (OCR) and ECAR. Approximately 20,000 cells were seeded in 96-well Seahorse cell culture plates (Seahorse XF96 V3 PS Cell Culture Microplates, 101085-004, Agilent Technologies) and pretreated for 15 h overnight with cytokines. The medium of cells was changed after one washing step 1 h before the assay to plain Dulbecco's modified Eagle medium (DMEM, D5030, Sigma-Aldrich) titrated to pH 7.4 and supplemented with 10 mM glucose (Seahorse XF 1.0 M glucose solution, 103577-100, Agilent Technologies), 2 mM glutamine (Seahorse XF 200 mM glutamine solution, 103579-100, Agilent Technologies) and 10 mM HEPES. A typical injection strategy for the mitochondrial stress test was performed by injecting oligomycin (495455, Sigma-Aldrich) first, followed by carbonyl cyanide-p-trifluoromethoxyphenylhydrazone (FCCP, C2920, Sigma-Aldrich), and finally antimycin A (A8674, Sigma-Aldrich) and rotenone (R8875, Sigma-Aldrich). The final concentration for oligomycin was 20 µM, 1.25 µM for FCCP and 2 µM for antimycin A and rotenone. The gathered data were normalized by the cell count in each well measured by CyQUANT Cell Proliferation Assay and the average of cells in the EBM control group wells as reference. The smallest measurement of OCR after the last injection defined the non-mitochondrial oxygen consumption. The baseline was determined by the lowest measurement of OCR before oligomycin injection, subtracted from the non-mitochondrial oxygen consumption. ATP production-related OCR was calculated by the difference between the baseline and the lowest measurement following oligomycin injection. Finally, the highest OCR after FCCP injection subtracted from non-mitochondrial oxygen consumption defined the maximum respiration.

Co-staining of STAT3 and mitochondria

Plasmids coding for Venus1–STAT3 [Venus1-WTSTAT3 (Letra-Vilela et al., 2020), 123164, Addgene] and Venus2–STAT3 [Venus2-WTSTAT3 (Letra-Vilela et al., 2020), 123165, Addgene] were purchased and transformed in bacteria following the One Shot Stbl3 (C737303, Thermo Fisher Scientific) protocol. Then, 1 ml of the generated stock solution was plated on agar plates and grown overnight in the incubator. Plasmids were isolated using the Plasmid DNA Purification Mini Prep Kit (S5369.0050, Genaxxon BioScience, Ulm, Germany). For quality control, plasmids were digested using the enzymes BrsGI (R0575S, New England Biolabs) and NotI (R0189S, New England Biolabs) according to the protocol generated for these enzymes by NEBcloner (https://nebcloner.neb.com/#!/protocol/re/double/BsrGI,NotI). The plasmid fragments were amplified by standard PCR and DNA was detected on a 1% agarose gel.

For transfection experiments, BAECs (GM-7373, Leibniz Institut – German Collection of Microorganisms and Cell Cultures, Leipzig, Germany) cultured on fibronectin-coated flasks (Human Plasma Fibronectin Purified Protein, FC010, Merck, Darmstadt, Germany) were used. BAECs were transfected with the plasmids encoding Venus1–STAT3 (1.04 ng/µl) and Venus2–STAT3 (1.04 ng/µl) in 8.3% Lipofectamine 2000 (11668030, Thermo Fisher Scientific)-containing medium. After 24 h, the cells were stimulated with cytokines for 30 min, then fixed with 2% paraformaldehyde for 20 min and blocked with 10% goat serum (005-000-121, Jackson ImmunoResearch Laboratories) for 1 h. Cells were stained by MitoTracker Orange CMTMRos (M7510, Thermo Fisher Scientific) following the recommended protocol using a 1:3000 dilution. A Leica TCS SP8 confocal microscope and the LAS X 3.5.7 software generated high-quality representative images.

Mitochondrial assays

Reactive oxygen species (ROS) production following cytokine pretreatment overnight was measured using MitoSOX Red Mitochondrial Superoxide Indicator (M36008, Thermo Fisher Scientific). The signal was analyzed by a LSRFortessa flow cytometer (BD Bioscience). Debris and duplets were excluded from the analysis by gating using the FlowJo v10 software (FlowJo, Becton Dickinson, Franklin Lakes, NJ).

RNA sequencing

RNA isolation and all steps necessary for total RNA sequencing were conducted by Center of Excellence for Fluorescent Bioanalytics (KFB, University of Regensburg, Germany; www.kfb-regensburg.de). Samples were lysed in QIAzol and shipped on dry ice. Whole RNA was isolated using the RNeasy Micro Kit (74004, QIAGEN), including on-column DNase digestion and homogenization by Precellys CK14 ceramic beads (432-3751, VWR) before extraction. A combination of the Illumina TruSeq Stranded mRNA Sample Preparation Guide (TruSeq Stranded mRNA, 20020594, Illumina) and the Illumina NextSeq 2000 Sequencing System was used for library preparation and processing samples. Equimolar amounts of each library quantified by the KAPA Library Quantification (ABI Prism, KK4835, Roche Sequencing Solutions, Basel, Switzerland) were sequenced on a NextSeq 2000 instrument controlled by the NextSeq 2000 Control Software v1.1.0.27334, using two 100-cycle P2 Flow Cells with the single-index, single-read run parameters. Base calling and imaging analysis were done by the Real Time Analysis software v3.6.14. Resulting CBCL files were converted into FASTQ files with the bcl2fastq conversion software v2.20.

Bioinformatics

Raw data were uploaded to the European Galaxy server (https://usegalaxy.eu) for further analysis (Afgan et al., 2018). FastQC (Galaxy Version 0.72) (https://www.bioinformatics.babraham.ac.uk/projects/fastqc/) provided quality assessment of all raw files and STAR aligner (Galaxy Version 2.7.5b) (Dobin et al., 2012) mapped all reads to a human reference genome provided by GENCODE (GRCh38, release date 03.2020). The aligned reads were assigned to specific genes by featureCounts (Galaxy Version 1.6.4) (Liao et al., 2013) using the annotation file provided by GENCODE for the same reference genome. Standard settings were applied for all tools. Downstream analysis was performed in R 4.0.2 (https://www.r-project.org) by normalizing counts using the DESeq2 package (Love et al., 2014). Ensembl IDs (v101) were matched to HGNC gene abbreviations by BioMart (Durinck et al., 2009). Genes were considered to be differentially expressed at strict thresholds of adjusted P-value (P_{adj})<0.05 using the Benjamini–Hochberg method and an absolute $\log_2$(fold change)>1. GO enrichment analysis was conducted by the clusterProfiler R package (Yu et al., 2012), pathway enrichment analysis using the Reactome database by ReactomePA (Yu and He, 2016) and GSEA by ranking for shrinked $\log_2$(fold change) by fgsea (Sergushichev, 2016 preprint) and MSigDB gene sets for GO terms (Liberzon et al., 2011; downloaded 8 April 2021).

Statistics

Error bars show mean±s.e.m. Statistical testing was performed by a Mann–Whitney test or, when multiple samples were compared, a Kruskal–Wallis test adjusted for multiple testing using the methods described by Benjamini, Krieger and Yekutieli (Benjamini et al., 2006). P<0.05 was considered significant and marked with an asterisk. P<0.01 was visualized by two asterisks and P<0.001 by three asterisks.

Acknowledgements

We thank Patrick Metzger and Melanie Börries from the Institute of Medical Bioinformatics and Systems Medicine, Medical Center, University of Freiburg for advice concerning analysis of sequencing data. We would like to acknowledge the Lighthouse Core Facility, Medical Center, University of Freiburg for their assistance with the migration assay and flow cytometry by providing and maintaining the specific equipment, and the Kompetenzzentrum Fluoreszente Bioanalytik, Regensburg for sequencing services.

Competing interests

F.B. has the following potential conflicts of interest to declare: funding for scientific research projects from Roche and Neurotech pharmaceuticals; and speaker activity for Novartis and Bayer.

Author contributions

Conceptualization: J.R., O. Gorka, C.L., G.S., F.B.; Methodology: J.R., R.F.U.K.; Validation: J.R., M.J., F.B.; Formal analysis: J.R., M.J., J.W., J.A., O. Gorka, F.B.; Investigation: J.R., J.A.; Resources: J.R.; Data curation: J.R., J.W., F.B.; Writing - original draft: J.R., F.B.; Writing - review & editing: J.R., J.W., O. Gorka, C.L., H.A., G.S., F.B.; Visualization: J.R.; Supervision: O. Groß, C.L., H.A., G.S., F.B.; Project administration: G.S., F.B.; Funding acquisition: J.R., O. Gorka, O. Groß, F.B.

Funding

This work was supported by the Deutsche Forschungsgemeinschaft (Bu3135/3-1 to F.B.; CRC 850, project C09 to R.F.U.K.; and SFB 1160, SFB/TRR 167, SFB 1425, SFB 1479, GRK 2606 and CIBSS – EXC-2189 – project ID 390939984 to O. Groß), the Retinologische Gesellschaft, Germany (Dr. Werner-Jackstädt-Nachwuchspreis to F.B.), the Medizinische Fakultät der Albert-Ludwigs-Universität Freiburg (Berta-Ottenstein-Program for Clinician Scientists and Advanced Clinician Scientists to F.B.; MOTI-VATE Program to J.R.) and the European Research Council (337689 and 966687 to O. Groß).

Data availability

RNA sequencing data have been deposited to the Gene Expression Omnibus with the accession numbers GSE196776 and GSE198484.

Peer review history

The peer review history is available online at https://journals.biologists.com/jcs/article-lookup/doi/10.1242/jcs.260182.reviewer-comments.pdf.

References

Abe, H., Takeda, N., Isagawa, T., Semba, H., Nishimura, S., Morioka, M. S., Nakagama, Y., Sato, T., Soma, K., Koyama, K. et al. (2019). Macrophage hypoxia signaling regulates cardiac fibrosis via Oncostatin M. *Nat. Commun.* **10**, 2824. doi:10.s41467-020-1766/s41467-019-10859-w

Afgan, E., Baker, D., Batut, B., van den Beek, M., Bouvier, D., Čech, M., Chilton, J., Clements, D., Coraor, N., Grüning, B. A. et al. (2018). The Galaxy platform for accessible, reproducible and collaborative biomedical analyses: 2018 update. *Nucleic Acids Res.* **46**, W537-W544. doi:biomet/nar/gky379

Avalle, L. and Poli, V. (2018). Nucleus, mitochondrion, or reticulum? STAT3 à La Carte. *Int. J. Mol. Sci.* **19**, 2820. doi:10.3390/ijms19092820

Balic, J. J., Albargy, H., Luu, K., Kirby, F. J., Jayasekara, W. S. N., Mansell, F., Garama, D. J., De Nardo, D., Baschuk, N., Louis, C. et al. (2020). STAT3 serine phosphorylation is required for TLR4 metabolic reprogramming and IL-1β

expression. *Nat. Commun.* **11**, 3816. doi:10.s41467-020-1766/s41467-020-17669-5

Benjamini, Y., Krieger, A. M. and Yekutieli, D. (2006). Adaptive linear step-up procedures that control the false discovery rate. *biometrika* **93**, 491-507. doi:10.1093/biomet/93.3.491

Bucher, F., Walz, J. M., Bühler, A., Aguilar, E., Lange, C., Diaz-Aguilar, S., Martin, G., Schlunck, G., Agostini, H., Friedlander, M. et al. (2016). CNTF attenuates vasoproliferative changes through upregulation of SOCS3 in a mouse-model of oxygen-induced retinopathy. *Invest. Ophthalmol. Vis. Sci.* **57**, 4017-4026. doi:10.1167/iovs.15-18508

Bucher, F., Aguilar, E., Marra, K. V., Rapp, J., Arnold, J., Diaz-Aguilar, S., Lange, C., Agostini, H., Schlunck, G., Stahl, A. et al. (2020). CNTF prevents development of outer retinal neovascularization through upregulation of CxCl10. *Invest. Ophthalmol. Vis. Sci.* **61**, 20. doi:10.1167/iovs.61.10.20

Camaré, C., Pucelle, M., Nègre-Salvayre, A. and Salvayre, R. (2017). Angiogenesis in the atherosclerotic plaque. *Redox. Biol.* **12**, 18-34. doi:10.1016/j.redox.2017.01.007

Carbognin, E., Betto, R. M., Soriano, M. E., Smith, A. G. and Martello, G. (2016). Stat3 promotes mitochondrial transcription and oxidative respiration during maintenance and induction of naive pluripotency. *EMBO J.* **35**, 618-634. doi:10.15252/embj.201592629

Crawford, T. N., Alfaro, D. V., III, Kerrison, J. B. and Jablon, E. P. (2009). Diabetic retinopathy and angiogenesis. *Curr. Diabetes Rev.* **5**, 8-13. doi:10.2174/157339909787314149

Dan-Brezis, I., Zahavi, A., Axer-Siegel, R., Nisgav, Y., Dahbash, M., Weinberger, D., Ehrlich, R. and Livnat, T. (2019). Inflammation, angiogenesis and coagulation interplay in a variety of retinal diseases. *Acta Ophthalmol.* **98**, e559-e562. doi:10.1111/aos.14331

Davis, S., Aldrich, T. H., Valenzuela, D. M., Wong, V. V., Furth, M. E., Squinto, S. P. and Yancopoulos, G. (1991). The receptor for ciliary neurotrophic factor. *Science* **253**, 59-63. doi:10.1126/science.1648265

Davis, S., Aldrich, T. H., Ip, N. Y., Stahl, N., Scherer, S., Farruggella, T., Distefano, P., Curtis, R., Panayotatos, N., Gascan, H. et al. (1993). Released form of CNTF receptor alpha component as a soluble mediator of CNTF responses. *Science* **259**, 1736-1739. doi:10.1126/science.7681218

Deveza, L., Choi, J. and Yang, F. (2012). Therapeutic angiogenesis for treating cardiovascular diseases. *Theranostics* **2**, 801-814. doi:10.7150/thno.4419

Dobin, A., Davis, C. A., Schlesinger, F., Drenkow, J., Zaleski, C., Jha, S., Batut, P., Chaisson, M. and Gingeras, T. R. (2012). STAR: ultrafast universal RNA-seq aligner. *Bioinformatics* **29**, 15-21. doi:biomet/bioinformatics/bts635

Durinck, S., Spellman, P. T., Birney, E. and Huber, W. (2009). Mapping identifiers for the integration of genomic datasets with the R/Bioconductor package biomaRt. *Nat. Protoc.* **4**, 1184-1191. doi:10.1038/nprot.2009.97

Gough, D. J., Corlett, A., Schlessinger, K., Wegrzyn, J., Larner, A. C. and Levy, D. E. (2009). Mitochondrial STAT3 supports Ras-dependent oncogenic transformation. *Science* **324**, 1713-1716. doi:10.1126/science.1171721

Gough, D. J., Marié, I. J., Lobry, C., Aifantis, I. and Levy, D. E. (2014). STAT3 supports experimental K-RasG12D–induced murine myeloproliferative neoplasms dependent on serine phosphorylation. *Blood* **124**, 2252-2261. doi:10.1182/blood-2013-02-484196

Hanlon, M. M., Rakovich, T., Cunningham, C. C., Ansboro, S., Veale, D. J., Fearon, U. and McGarry, T. (2019). STAT3 mediates the differential effects of Oncostatin M and TNFα on RA synovial fibroblast and endothelial cell function. *Front. Immunol.* **10**, 2056. doi:10.3389/fimmu.2019.02056

Heinrich, P. C., Behrmann, I., Haan, S., Hermanns, H. M., Müller-Newen, G. and Schaper, F. (2003). Principles of interleukin (IL)-6-type cytokine signalling and its regulation. *Biochem. J.* **374**, 1-20. doi:10.1042/bj20030407

Hu, Y. S., Han, X. and Liu, X. H. (2019). STAT3: a potential drug target for tumor and inflammation. *Curr. Top. Med. Chem.* **19**, 1305-1317. doi:10.2174/1568026619666190620145052

Huang, S., Bucana, C. D., Van Arsdall, M. and Fidler, I. J. (2002). Stat1 negatively regulates angiogenesis, tumorigenicity and metastasis of tumor cells. *Oncogene* **21**, 2504-2512. doi:10.1038/sj.onc.1205341

Jiang, B. H. and Liu, L. Z. (2008). AKT signaling in regulating angiogenesis. *Curr. Cancer Drug Targets* **8**, 19-26. doi:10.2174/156800908783497122

Johnson, D. E., O'Keefe, R. A. and Grandis, J. R. (2018). Targeting the IL-6/JAK/STAT3 signalling axis in cancer. *Nat. Rev. Clin. Oncol.* **15**, 234-248. doi:10.1038/nrclinonc.2018.8

Jones, S. A. and Jenkins, B. J. (2018). Recent insights into targeting the IL-6 cytokine family in inflammatory diseases and cancer. *Nat. Rev. Immunol.* **18**, 773-789. doi:10.1038/s41577-018-0066-7

Jung, J. E., Lee, H. G., Cho, I. H., Chung, D. H., Yoon, S. H., Yang, Y. M., Lee, J. W., Choi, S., Park, J. W., Ye, S. K. et al. (2005). STAT3 is a potential modulator of HIF-1-mediated VEGF expression in human renal carcinoma cells. *FASEB J.* **19**, 1296-1298. doi:10.1096/fj.04-3099fje

Jung, I., Jung, D., Zha, Z., Jeong, J., Noh, S., Shin, J., Park, J.-K., Kim, K.-S., Jeong, Y., Hur, J. et al. (2021). Interferon-γ inhibits retinal neovascularization in a mouse model of ischemic retinopathy. *Cytokine* **143**, 155542. doi:10.1016/j.cyto.2021.155542

Kucia-Tran, J. A., Tulkki, V., Scarpini, C. G., Smith, S., Wallberg, M., Paez-Ribes, M., Araujo, A. M., Botthoff, J., Feeney, M., Hughes, K. et al. (2018). Anti-oncostatin M antibody inhibits the pro-malignant effects of oncostatin M receptor overexpression in squamous cell carcinoma. *J. Pathol.* **244**, 283-295. doi:10.1002/path.5010

Letra-Vilela, R., Cardoso, B., Silva-Almeida, C., Maia Rocha, A., Murtinheira, F., Branco-Santos, J., Rodriguez, C., Martin, V., Santa-Marta, M. and Herrera, F. (2020). Can asymmetric post-translational modifications regulate the behavior of STAT3 homodimers? *FASEB Bioadv.* **2**, 116-125. doi:10.1096/fba.2019-00049

Liao, Y., Smyth, G. K. and Shi, W. (2013). featureCounts: an efficient general purpose program for assigning sequence reads to genomic features. *Bioinformatics* **30**, 923-930. doi:10.1093/bioinformatics/btt656

Liberzon, A., Subramanian, A., Pinchback, R., Thorvaldsdóttir, H., Tamayo, P. and Mesirov, J. P. (2011). Molecular signatures database (MSigDB) 3.0. *Bioinformatics* **27**, 1739-1740. doi:10.1093/bioinformatics/btr260

Love, M. I., Huber, W. and Anders, S. (2014). Moderated estimation of fold change and dispersion for RNA-seq data with DESeq2. *Genome Biol.* **15**, 550. doi:10.1186/s13059-014-0550-8

Melincovici, C. S., Boşca, A. B., Şuşman, S., Mărginean, M., Mihu, C., Istrate, M., Moldovan, I. M., Roman, A. L. and Mihu, C. M. (2018). Vascular endothelial growth factor (VEGF) - key factor in normal and pathological angiogenesis. *Rom. J. Morphol. Embryol.* **59**, 455-467.

Mikhailov, A. and Gundersen, G. G. (1998). Relationship between microtubule dynamics and lamellipodium formation revealed by direct imaging of microtubules in cells treated with nocodazole or taxol. *Cell Motil. Cytoskeleton* **41**, 325-340. doi:10.1002/(SICI)1097-0169(1998)41:4<325::AID-CM5>3.0.CO;2-D

Modur, V., Feldhaus, M. J., Weyrich, A. S., Jicha, D. L., Prescott, S. M., Zimmerman, G. A. and McIntyre, T. M. (1997). Oncostatin M is a proinflammatory mediator. In vivo effects correlate with endothelial cell expression of inflammatory cytokines and adhesion molecules. *J. Clin. Invest.* **100**, 158-168. doi:10.1172/JCI119508

Navaratna, D., Guo, S., Arai, K. and Lo, E. H. (2009). Mechanisms and targets for angiogenic therapy after stroke. *Cell Adhes. Migr.* **3**, 216-223. doi:10.4161/cam.3.2.8396

Ng, D. C. H., Lin, B. H., Lim, C. P., Huang, G., Zhang, T., Poli, V. and Cao, X. (2006). Stat3 regulates microtubules by antagonizing the depolymerization activity of stathmin. *J. Cell Biol.* **172**, 245-257. doi:10.1083/jcb.200503021

Potente, M. and Carmeliet, P. (2017). The Link Between Angiogenesis and Endothelial Metabolism. *Annu. Rev. Physiol.* **79**, 43-66. doi:10.1146/annurev-physiol-021115-105134

Richards, C. D. (2013). The enigmatic cytokine oncostatin m and roles in disease. *ISRN Inflamm.* **2013**, 512103. doi:10.1155/2013/512103

Sergushichev, A. A. (2016). An algorithm for fast preranked gene set enrichment analysis using cumulative statistic calculation. *bioRxiv*, 060012. doi:10.1101/060012

Sun, D., Li, S., Wu, H., Zhang, M., Zhang, X., Wei, L., Qin, X. and Gao, E. (2015). Oncostatin M (OSM) protects against cardiac ischaemia/reperfusion injury in diabetic mice by regulating apoptosis, mitochondrial biogenesis and insulin sensitivity. *J. Cell. Mol. Med.* **19**, 1296-1307. doi:10.1111/jcmm.12501

Teng, T. S., Lin, B., Manser, E., Ng, D. C. H. and Cao, X. (2009). Stat3 promotes directional cell migration by regulating Rac1 activity via its activator βPIX. *J. Cell Sci.* **122**, 4150-4159. doi:10.1242/jcs.057109

Timofeeva, O. A., Chasovskikh, S., Lonskaya, I., Tarasova, N. I., Khavrutskii, L., Tarasov, S. G., Zhang, X., Korostyshevskiy, V. R., Cheema, A., Zhang, L. et al. (2012). Mechanisms of unphosphorylated STAT3 transcription factor binding to DNA. *J. Biol. Chem.* **287**, 14192-14200. doi:10.1074/jbc.M111.323899

Vasse, M., Pourtau, J., Trochon, V., Muraine, M., Vannier, J.-P., Lu, H., Soria, J. and Soria, C. (1999). Oncostatin M induces angiogenesis in vitro and in vivo. *Arterioscler. Thromb. Vasc. Biol.* **19**, 1835-1842. doi:10.1161/01.ATV.19.8.1835

Viallard, C. and Larrivée, B. (2017). Tumor angiogenesis and vascular normalization: alternative therapeutic targets. *Angiogenesis* **20**, 409-426. doi:10.1007/s10456-017-9562-9

Wegrzyn, J., Potla, R., Chwae, Y.-J., Sepuri, N. B., Zhang, Q., Koeck, T., Derecka, M., Szczepanek, K., Szelag, M., Gornicka, A. et al. (2009). Function of mitochondrial Stat3 in cellular respiration. *Science* **323**, 793-797. doi:10.1126/science.1164551

Wolf, D. and Ley, K. (2019). Immunity and Inflammation in Atherosclerosis. *Circ. Res.* **124**, 315-327. doi:10.1161/CIRCRESAHA.118.313591

Yu, G. and He, Q.-Y. (2016). ReactomePA: an R/Bioconductor package for reactome pathway analysis and visualization. *Mol. Biosyst.* **12**, 477-479. doi:10.1039/C5MB00663E

Yu, G., Wang, L.-G., Han, Y. and He, Q.-Y. (2012). clusterProfiler: an R package for comparing biological themes among gene clusters. *OMICS: A J. Integr. Biol.* **16**, 284-287. doi:10.1089/omi.2011.0118

Zhang, Q., Raje, V., Yakovlev, V. A., Yacoub, A., Szczepanek, K., Meier, J., Derecka, M., Chen, Q., Hu, Y., Sisler, J. et al. (2013). Mitochondrial localized Stat3 promotes breast cancer growth via phosphorylation of serine 727. *J. Biol. Chem.* **288**, 31280-31288. doi:10.1074/jbc.M113.505057

Zhang, X., Zhu, D., Wei, L., Zhao, Z., Qi, X., Li, Z. and Sun, D. (2015). OSM enhances angiogenesis and improves cardiac function after myocardial infarction. *BioMed Res. Int.* **2015**, 317905. doi:10.1155/2015/317905

Zhang, Q., Lu, S., Li, T., Yu, L., Zhang Y., Zeng, H., Qian, X., Bi, J. and Lin, Y. (2019). ACE2 inhibits breast cancer angiogenesis via suppressing the VEGFa/VEGFR2/ERK pathway. *J. Exp. Clin. Cancer Res.* **38**, 173. doi:10.1186/s13046-019-1156-5

Zhu, M., Che, Q., Liao, Y., Wang, H., Wang, J., Chen, Z., Wang, F., Dai, C. and Wan, X. (2015). Oncostatin M activates STAT3 to promote endometrial cancer invasion and angiogenesis. *Oncol. Rep.* **34**, 129-138. doi:10.3892/or.2015.3951